

# Aerodynamic roughness length of crevassed tidewater glaciers from UAV mapping

Armin Dachauer<sup>1,2</sup>, Richard Hann<sup>3</sup>, and Andrew J. Hodson<sup>2,4</sup>

<sup>1</sup>Swiss Federal Institute of Technology in Zurich (ETH), Zurich, Switzerland

<sup>2</sup>The University Centre in Svalbard (UNIS), Longyearbyen, Svalbard

<sup>3</sup>Norwegian University of Science and Technology (NTNU), Trondheim, Norway

<sup>4</sup>Western Norway University of Applied Sciences, Sogndal (HVL), Norway

**Correspondence:** Armin Dachauer (armin.dachauer@bluewin.ch) and Richard Hann (richard.hann@ntnu.no)

**Abstract.** The aerodynamic roughness length ( $z_0$ ) is an important parameter in the bulk approach for calculating turbulent fluxes and their contribution to ice melt. However,  $z_0$  estimates for heavily crevassed tidewater glaciers  ~~$z_0$  estimations~~ are rare or only generalized. This study used unmanned aerial vehicles (UAVs) to map inaccessible tidewater glacier front areas. The high-resolution images were ~~used~~ utilized in a structure-from-motion photogrammetry approach to build digital elevation models (DEMs). These DEMs were applied to five ~~different~~ models (split across transect and raster methods) to estimate  $z_0$  values of the mapped area. The results point out that the range of  $z_0$  values across a crevassed glacier is large, with up to three ~~(locally even four)~~ orders of magnitude. The division of the mapped area into sub-grids (50 m  $\times$  50 m), each producing one  $z_0$  value, ~~best~~ accounts for the high spatial variability of  $z_0$  across the glacier. The  $z_0$  ~~estimations~~ estimates from the transect method are in general ~~higher~~ greater (up to one order of magnitude) than the raster method ~~estimations~~ estimates. Furthermore, wind direction (values parallel to the ice flow direction are ~~larger than perpendicular~~ greater than perpendicular values) and the chosen sub-grid size turned out to have a large impact on the  $z_0$  values, again presenting a range of up to one order of magnitude each. On average,  $z_0$  values between 0.08 m and 0.88 m for a down-glacier wind direction were found. The UAV approach proved to be an ideal tool to provide distributed  $z_0$  ~~estimations~~ estimates of crevassed glaciers, which can be incorporated by models to improve the prediction of turbulent heat fluxes and ice melt rates.

## 1 Introduction

The aerodynamic roughness of a glacier influences the turbulent heat exchange between the glacier surface and the atmosphere (Rees and Arnold, 2006). Both sensible and latent heat fluxes ~~balance~~ lead to this heat exchange on the surface and therefore have a large impact on the meltwater production and the surface energy balance of glaciers (Hock, 2005). The bulk ~~aerodynamic method is a very popular~~ approach for the calculation of those turbulent fluxes is very popular due to its low requirements for data collection. It only requires basic atmospheric measurements (e.g. wind speed, temperature) as well as the aerodynamic roughness length of the surface (Chambers et al., 2020). The aerodynamic roughness length, also called  $z_0$ , is a length scale that represents the height above the surface at which the wind speed drops to zero (Chappell and Heritage, 2007). It is a ~~constant surface characteristics (Lettau, 1969) describing~~ surface characteristics and therefore independent of meteorological quantities

(Lettau, 1969). In more detail,  $z_0$  describes the loss of wind momentum that can be attributed to surface roughness (Smith, 25 2014).

Recently, a series of studies (e.g. Irvine-Fynn et al., 2014; Miles et al., 2017; Smith et al., 2016) ~~were following the bulk approach to determine~~ have determined  $z_0$  values of glacier surfaces based on the bulk approach while using digital elevation models (DEMs) as ~~data source for their calculation~~ calculation data source. Terrestrial Light Detection and Ranging (LiDAR) systems (used for instance in the studies of Smith et al. (2016), Nicholson et al. (2016) or Nield et al. (2013a)) constitute a 30 powerful way to effectively produce such DEMs. However, they are very expensive (Uysal et al., 2015) and limited in the area they cover (Irvine-Fynn et al., 2014). Thus, unmanned aerial vehicles (UAVs), often also called uncrewed vehicle systems or drones, provide a cheap alternative to overcome these limitations (Uysal et al., 2015) because they are more flexible in their use and less limited by local topology as they provide a bird's-eye perspective. In recent years, UAVs have presented new opportunities for detailed mapping of the earth surface and ~~became~~ have become more and more popular in the field of 35 glaciology (Bhardwaj et al., 2016). The main advantage of UAVs is the possibility of collecting high temporal and spatial resolution data at low costs (Casella and Franzini, 2016) and to overcome the gap between sparse field observations and coarse resolution space-born remote sensing data (Bhardwaj et al., 2016).

Several studies already investigated the  $z_0$  values of non-crevassed (Irvine-Fynn et al., 2014; Nield et al., 2013a), debris-covered (Quincey et al., 2017) ~~or~~, sparsely crevassed (Smith et al., 2016) or rough (van Tiggelen et al., 2021) glacier ice sur- 40 faces using different approaches. However, still little is known about the effect of heavily crevassed glacier surfaces on the turbulent heat exchange between glaciers and the atmosphere. ~~The greatly varying size~~ A broader-scale, heterogeneous surface topography of obstacles (i.e. crevasses) ~~and the broader-scale, heterogeneous surface topography of such crevassed ice makes it hard to define~~ makes the definition of  $z_0$  values challenging (Quincey et al., 2017). Typical values of  $z_0$  on glacier ice range from less than 0.0001 m for smooth ice and 0.02 m to 0.08-0.1 m for rough glacier ice (~~Brock et al., 2006; Smeets et al., 1999~~) 45 ~~But~~ (Brock et al., 2006; Smeets et al., 1999; van Tiggelen et al., 2021), but published  $z_0$  ~~literature~~ values for large and deep crevasses are rare. Table 1 gives a closer overview of such published aerodynamic roughness values and shows  $z_0$  values up to 0.5 m for large crevasses (Fitzpatrick et al., 2019). Furthermore, most surface energy balance models only consider one single  $z_0$  value for the whole glacier (commonly 0.001 m (Smith et al., 2020)), regardless of any spatial and temporal variability (Quincey et al., 2017). The aerodynamic roughness length is a key parameter for the calculation of turbulent fluxes (Chambers 50 et al., 2020) ~~since~~ a change in  $z_0$  by an order of magnitude can double the estimated turbulent fluxes (Brock et al., 2006; Munro, 1989). The uncertainty in  $z_0$  values therefore presents a serious challenge for the calculation of surface ice melt (Smith et al., 2016) and its accurate parameterization is crucial, especially for complex ice surfaces, ~~is crucial (Quincey et al., 2017)~~.

The objective of this study is to assess the application of UAVs for capturing spatially variable  $z_0$  values of heavily crevassed ice surfaces. A photogrammetry method is used to build DEMs of the mapped glaciers from the aerial images, which are then 55 utilized to estimate the aerodynamic roughness length of crevassed tidewater glaciers in Svalbard. The main advantage of this approach is that increasingly available UAV technology is can be used to estimate turbulent fluxes that are usually difficult to measure in the field. Furthermore, the chosen DEM approach allows glaciers to be divided into areas of different aerodynamic

**Table 1.** Published aerodynamic roughness length values for crevassed glacier areas.

Study	Method	Surface Type	$z_0$ (m)
Fitzpatrick et al. (2019)	Raster	Large crevasses	0.01-0.5
Obleitner (2000)	Transect	Very rough glacier ice	0.05
Smeets et al. (1999)	Transect	Very rough glacier ice	0.02-0.08
Smith et al. (2016)	Transect	Deep crevasses	0.005-0.05
Smith et al. (2016)	Raster	Deep crevasses	0.003-0.025

roughness length values, leading to a better spatial representation of the turbulent fluxes and therefore surface ice melt on glaciers.

60 **2 Data and methods**

The following section describes how a DEM was generated from aerial imagery of crevassed glaciers in Svalbard. Images were obtained using off-the-shelf UAVs. In addition, different methods to calculate the aerodynamic roughness length from the DEMs are introduced.

**2.1 Field sites**

65 Four heavily crevassed tidewater ~~glaciers~~ glacier termini in Central Spitzbergen (see Fig. 1 and Table 2) were visited during three field campaigns. Nordenskiöldbreen was visited in summer 2019 and 2020. In spring 2020 further fieldwork was conducted on Fridtjovbreen, Heuglinbreen and Tunabreen. Fridtjovbreen is a single tidewater glacier of about 13 km length, flowing southwards and terminating in Van Mijenfjorden on the western side of Spitzbergen island. Here precipitation and temperature are relatively high with an annual temperature of about -4°C and precipitation of up to 1000 mm (Hanssen-Bauer  
70 et al., 2019). Both Nordenskiöldbreen and Tunabreen are outlet glaciers (flowing from northeast to southwest) draining the large Lomonosovfonna ice cap, where the precipitation usually is lower than on the west coast (Hagen et al., 1993). While Nordenskiöldbreen is a roughly 15 km long, wide tidewater glacier terminating in Billefjorden, Tunabreen is narrower, with a length of about 20 km and terminating in Tempelfjorden. Additionally, both Tunabreen and Fridtjovbreen are known to have experienced a ~~surging~~ surge event. While the surge on Fridtjovbreen already happened during the 1990s (Murray et al., 2012),  
75 Tunabreen surged more recently in the years 2003 to 2005 and had another advance of the glacier front about ten years later (Ericson et al., 2019). Heuglinbreen is a tidewater glacier flowing southwards and terminating into Mohnbukta, a bay on the east coast of Spitzbergen. This region is known to be particularly cold (annual temperature of about -10°C) and ~~rather~~ dry (annual precipitation up to 700 mm) (Hanssen-Bauer et al., 2019).

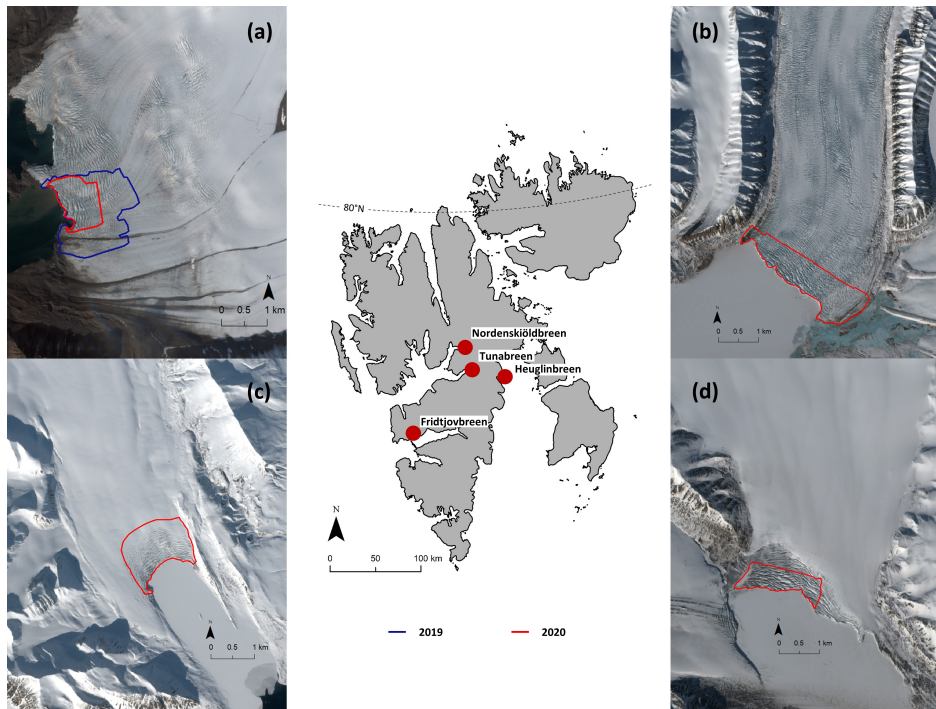


**Figure 1.** Field sites: Map of Svalbard with marked locations of the investigated tidewater glaciers (red dots). Additionally, Sentinel-2 satellite images (ESA, 2020) of the glaciers Nordenskiöldbreen (a), Tunabreen (b), Fridtjovbreen (c) and Heuglinbreen (d) taken at the according week of fieldwork provide a closer look. The lines mark the mapped front area for each glacier in 2019 (blue) and 2020 (red).

## 2.2 Field data collection

80 UAV-based aerial imagery was collected during each fieldwork campaign with off-the-shelf UAVs (a DJI Mavic 2 Enterprise and a DJI Phantom 4 Pro). In order to have a sufficient resolution of the crevasse fields, a target DEM-resolution of about 0.25 m/px was chosen. To achieve this DEM resolution, the UAV imagery aimed for a ground sampling distance (GSD) of at least 0.1 m/px, a forward overlap of 90 %, and a side overlap of 80 %. During fieldwork the UAVs were planned to operate at an altitude of 200 m above ground-level, taking nadir-viewing pictures. Flights were conducted with pre-programmed waypoints and a  
85 run separation of 70 m. Since information about the glacier surface elevation was unknown to the UAV, the true altitude above the glacier surface was typically less than 200 m. As a result, the GSD ranged between 0.04 - 0.07 m/px and the subsequent DEM resolution ranged between 0.17 to 0.28 m/px (see Table 2).

## 2.3 DEM generation and preparation

The high-resolution images from the UAVs were processed with a structure-from-motion (SfM) multi-view stereo (MVS) photogrammetry method using Agisoft Metashape version 1.6.2 (Agisoft LLC, 2020). Building DEMs in Agisoft is a three-step process: image alignment, construction of a dense cloud  $\bar{\rho}$  and DEM generation (Verhoeven, 2011). The software runs on

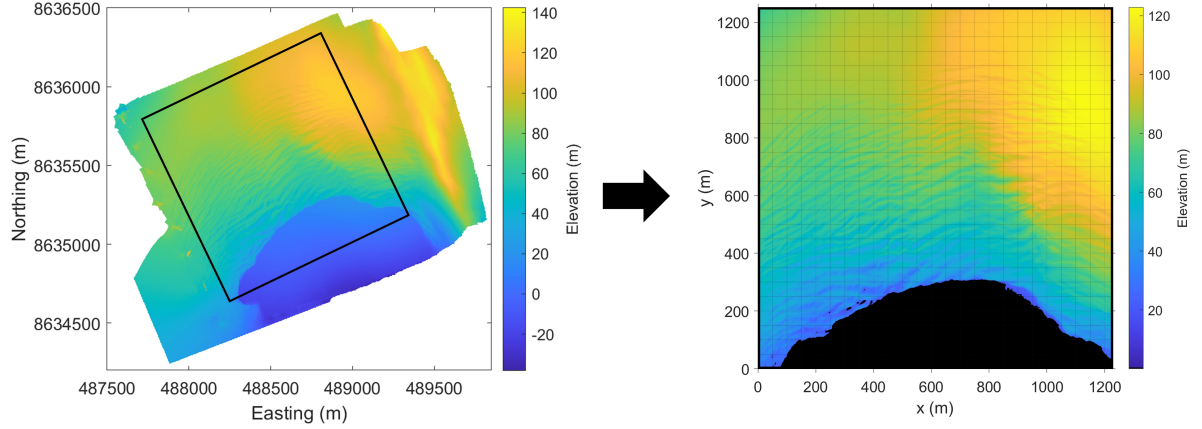
**Table 2.** Overview of the tidewater glaciers visited and the date of their UAV survey. Additionally, the size of the mapped area and DEM resolution ,as well as the average height and length of roughness elements for a up-/down-glacier (cross-glacier) wind direction are listed.

Glacier	Date	Location	Area (km <sup>2</sup> )	Res. (m/px)	Height (m)	Length (m)
Nordenskiöldbreen 2019	19.-22. August 2019	78°39' N, 17°00' E	2.6	0.17	10 (7)	29 (41)
Tunabreen	28. April 2020	78°27' N, 17°23' E	2.4	0.19	14 (11)	37 (43)
Heuglinbreen	04. May 2020	78°21' N, 18°47' E	1.1	0.21	14 (9)	31 (35)
Fridtjovbreen	07. May 2020	77°47' N, 14°31' E	1.0	0.28	8 (6)	29 (46)
Nordenskiöldbreen 2020	21. July 2020	78°39' N, 17°00' E	0.9	0.22	16 (9)	35 (49)

a fully automatically workflow. However, the whole processing comes along with many parameter settings that can be selected to improve the DEM quality depending on the input data and the output purpose. To determine an ideal set of parameters for our approach, many different combinations of settings were tested leading to the optimized final settings (see Dachauer  
95 (2020)). Due to an inaccessible glacier surface, no ground control points (GCPs) could be placed on the mapped area for georeferencing. No alternative georeferencing platforms such as real-time-kinematic correction (Chudley et al., 2019) were available. While this is a recommended procedure for future application of this technique, we point out that computation of  $z_0$  requires quantification of relative topographic differences and so the impact of this shortcoming is minor.

Before starting the model calculations of the aerodynamic roughness length, the DEMs obtained from the SfM processing  
100 were rotated in such a way that the glacier flow direction corresponds to the column alignment of the DEM, with the front at the lower part (see Fig. 2). This allowed the estimation of  $z_0$  values for ~~all-four-dominant-wind-directions(downwind,upwind,crosswinds)~~the following four wind directions: down-glacier, up-glacier and cross-glacier from both sides. Furthermore, the DEMs were cropped to a shape that contains the most crevassed zones. This area is specific to each glacier and varies significantly due to the differences in glacier size, time available for mapping, number of UAV batteries, and limitations due to GPS  
105 interference. The sea ice and water area in front of the glaciers was removed ~~,~~since it has no contribution to the turbulent heat exchange of the glacier.

This study assumes that the mean airflow is blowing parallel to the slope of the glacier. This means that the glacier slope has no effect on the aerodynamic roughness (Fitzpatrick et al., 2019). Furthermore, it ~~means-justifies the assumption~~ that the aerodynamic roughness is in the first place influenced by the macro-structure of the surface (crevasses, large obstacles,  
110 etc.) and not only by small-scale surface roughness on the crevasse obstacles. In other words, only looking at the small-scale surface roughness elements would lead to a wrong roughness parameterization since they might be located on the inner side of a large-scale roughness obstacle not exposed to the whole mean airflow. Accordingly, the ~~selected-chosen~~ grid size must be ~~selected-in-a-way-that-represents-this~~large enough to include the macro-structure of the surface ~~,~~since because small-scale roughness elements alone do not represent the real topographic expression. Linear detrending over long baselines manages to  
115 represent areas of high curvature (Smith, 2014) and is therefore appropriate for this purpose. Figure 3 presents the impact and importance of the chosen sub-grid size (i.e. length of detrended transect) on the modelled surface roughness. The blue line on



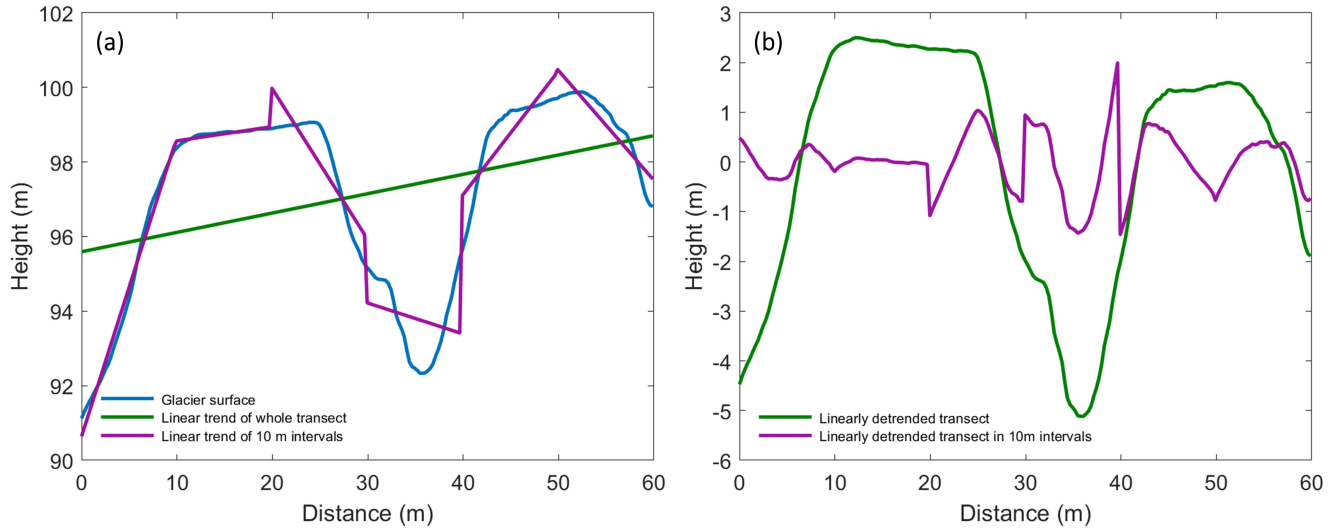
**Figure 2.** The originally mapped DEM (left) of Fridtjovbreen was rotated and cropped (black frame) before using it for the model calculations. Additionally, the elevation values of the sea ice area were removed and the whole DEM was divided into sub-grids of 50 m × 50 m (right).

Fig. 3 (a) shows a random transect of two roughness elements of 30 m width on Fridtjovbreen. Two linear detrending methods were applied to the surface data of this illustration. First, the green line detrended the whole transect. Second, the transect was detrended in 10 m intervals (purple line). The detrended data (Fig. 3 (b)) shows that the 10 m grid size only captured the small-scale surface roughness of the obstacles (purple line). In contrast, the linearly detrended transect length of 60 m (green line) managed to represent the two large roughness elements. Therefore, a sub-grid size of at least the width of an average obstacle should be chosen to account for the macro-structure surface roughness of the crevassed glaciers. On average, the mapped tidewater glaciers had obstacle widths between 30 m and 50 m (calculated according to the transect method of Munro (1989), see Table 2). Thus, the final DEMs were subdivided into rectangular sub-grids of 50 m × 50 m (grid in Fig. 2), each estimating one  $z_0$  value.

## 2.4 Models for aerodynamic roughness length estimation

The aerodynamic roughness length was calculated for each ~~sub-grid DEM and all DEM sub-grid and all four~~ wind directions with five models after 2D-linear detrending (see Fig. 3). The most common models in glaciology for calculating  $z_0$  using the bulk method are based on the work of Lettau (1969), who developed the following equation for the bulk aerodynamic roughness length:

$$z_0 = c_d h^* \frac{s}{S}, \quad (1)$$



**Figure 3.** Graph (a) shows a random transect of two roughness elements on Fridtjovbreen (blue line). The transect is linearly detrended, either over the whole profile (green) or in 10 m intervals (purple). Graph (b) illustrates the linearly detrended surface data applied at the whole transect (green line), or applied at 10 m intervals (purple line).

where  $h^*$  is the effective obstacle height (m),  $s$  is the silhouette or frontal area of the obstacle ( $m^2$ ) and  $S$  the horizontal ground area ( $m^2$ ). The value  $c_d = 0.5$ , first proposed by Lettau (1969), corresponds to the average drag coefficient of a characteristic roughness element.

135 The definition of the parameters of Equation 1 ~~turns out to be more difficult~~ is more complex in glacial environments ~~where since~~ the individual roughness elements ~~vary a lot~~ are non-uniform and vary substantially in height, size and density (Chambers et al., 2020). Therefore, the original equation has been adjusted and further developed in several studies, leading to the five different models used in this study (Table 3). The five models can be subdivided into two groups according to how they determine and measure roughness elements. One group counts the number of roughness elements in a transect (hereafter

140 called the 'transect method'), while the other group is based on a raster approach (hereafter called the 'raster method') using every DEM cell value for the calculation of  $z_0$ . The choice of the models is justified by comparing results of the two methods and to further give insights into the impact of variable parameterization on  $z_0$  estimates for each method.

Two models using the transect method were included in this study, only differing in their definition of the effective obstacle height  $h^*$  (m). Each row of the ~~detrended~~ sub-grid was ~~detrended~~ and treated as a separate transect of length  $X$  (m), whereof

145 the transition frequency  $f$  from below to above the mean elevation was recorded (often referred to as 'zero-up-crossing' in literature) for the calculation of the transect  $z_0$  value. Thus, the final  $z_0$  value for each sub-grid was then calculated by averaging the individual transect  $z_0$  values within the sub-grid. First, the Lettau model calculates  $h^*$  by taking the average vertical extent of the detrended roughness elements, as described by Lettau (1969). Second, the Munro model simplifies Equation 1 of Lettau (1969) such that the height of roughness element  $h^*$  is calculated by taking twice the standard deviation of elevations along the

**Table 3.** Overview of parameters from the Lettau (1969) Equation 1 used for the  $z_0$  calculation of each model.

Parameter	Smith	Chambers	Fitzpatrick	Munro	Lettau
Effective obstacle height $h^*$ (m)	Mean height above the detrended plane	$2 \times$ standard deviation of $z$ above detrended plane	Mean height above the detrended plane	$2 \times$ standard deviation of detrended profile	Mean obstacle height
Silhouette area $s$ (m <sup>2</sup> )	Frontal area above detrended plane across whole sub-grid calculated for all four wind direction		Frontal area across window above the height of the first row cells calculated for <del>each-all cardinal-wind-direction</del> <u>four wind directions</u>	Frontal area of a modelled roughness element: $h^* X/2f$ . With $X$ = transect length, $f$ = transition frequency	
Ground area $S$ (m <sup>2</sup> )	Full area of DEM sub-grid		Area of moving-window	Ground area of a modelled roughness element: $(X/f)^2$	
Drag coefficient $c_d$	0.5				
Roughness length $z_0$ (m)	$z_0 = c_d h^* \frac{s}{S}$				

150 detrended transect, as described by Munro (1989). In contrast to the study of Munro (1989), which used wind-perpendicular surface transects for the roughness calculation, we used wind-parallel profiles for both models of the transect method. This is because if a crevasse is aligned perpendicular to the prevailing wind direction, a wind-perpendicular transect is not able to detect the crevasse, yielding a relatively low  $z_0$  value (for further explanation see (Smith et al., 2016)). Thus, such an adaptation is essential for heterogeneous ~~roughness elements like crevasses which are naturally streamlined (Smith et al., 2016) and naturally~~  
155 streamlined roughness elements as those investigated in this study, since wind systems are influenced by the large-scale catchment topography and therefore often flow up or down the glacier (Quincey et al., 2017). The transect method presents a simple approximation of the roughness elements across a profile and, in contrast to the raster method, assumes all roughness elements to be of equal height, uniformly distributed, isotropic and not affected by any sheltering effects(~~Smith et al., 2016~~).

The raster method is ~~directly~~also based on the Lettau (1969) Equation 1 ~~and but~~ the elevation differences between two  
160 adjacent cells define the surface roughness ~~at in~~ the end. In the raster method all sub-grids were detrended row-wise and areas below the detrended plane were neglected, assuming that they would be effectively sheltered. Three models following the raster method were included in this study. First, the Smith model was based on the 'DEM-based' approach described by Smith et al. (2016). The effective obstacle height  $h^*$  was calculated as the mean elevation of all the cells of each row above the zero plane. The second model of the raster method (hereafter called Chambers model) was based on the 'DEM method' described  
165 by Chambers et al. (2020). Its only difference to the Smith model is again the definition of the effective obstacle height  $h^*$ , which is twice the standard deviation of elevations above the detrended plane. The third model of the raster method (hereafter

called Fitzpatrick model) was based on the 'Block estimation' described by Fitzpatrick et al. (2019). While the two previous raster methods calculated some of the parameters row-wise, this method followed a moving-window approach (see Table 3). The obstacle height  $h^*$  corresponded to the mean of all the detrended elevation values above the zero plane within the window. In this study, a window size of 30 m was chosen, which corresponded to the lower estimation of an average roughness element on the investigated glaciers (see Table 2). For all three models,  $s$  and  $h^*$  were calculated individually for each row of sub-grid (moving-window for the Fitzpatrick model, respectively). Accordingly, the ground area  $S$  was assigned to the area of the sub-grid (moving-window) and the final  $z_0$  value for each sub-grid then calculated by taking the mean of its row (moving-window) values.

### 3 Results

The DEMs obtained from the UAV-based imagery and processed with the SfM-MVS method illustrate that the crevasses of the mapped glaciers are in general aligned perpendicular to the glacier flow direction. The crevasses closer to the front are often deeper and larger in terms of spacing (width of crevasse opening) compared to crevasses located upstream the glacier (see Fig. 4). The DEMs were then used to calculate the aerodynamic roughness lengths with the two transect method models and the three raster method models. The results (e.g. Fig. 4, 6 and 7) show that the spatial variability of  $z_0$  values across the mapped area is up to three ~~(locally even four)~~ orders of magnitude. In general, the larger a roughness element the larger its aerodynamic roughness length. The ~~highest values were calculated with the~~ largest  $z_0$  values (decimeter to meter scale) were found close to the glacier front where crevasses are big and steep using the transect methods and for winds blowing parallel to the flow direction of the glacier. ~~Such values can be found close to the glacier front where crevasses are big and steep.~~ The lowest values (millimeter to centimeter scale) are estimated with the raster methods for smooth, crevasse-free ice and for cross-glacier wind directions.

#### 3.1 Model results

Figure 4 shows the estimated aerodynamic roughness length values for each of the five applied models for the down-glacier wind direction on Nordenskiöldbreen 2019. The results reveal that all models agree on the relative spatial  $z_0$  patterns across the glacier. Accordingly, for the flatter and less crevassed part (e.g. to the right of the mapped area on Nordenskiöldbreen) all models show lower sub-grid  $z_0$  values (red) compared to the heavily crevassed part close to the glacier front (yellow). To further investigate the relative agreement between the models a statistical correlation test on the  $z_0$  data of Nordenskiöldbreen (averaged ~~in all over all four~~ wind directions) was conducted. The correlation test showed that all models are strongly correlated to each other leading to  $R^2$  values of 0.877 and higher (Dachauer, 2020). A similar correlation ~~has also been observed on was~~ also observed for the other glaciers. While this indicates that the  $z_0$  values are correlated, it does not provide any conclusion about the quality of the individual models.

Figure 4 further illustrates that the absolute values of the models Munro and Lettau show ~~higher~~ greater roughness values on the same sub-grid than the other three models. In more detail, the Lettau model estimates are generally ~~higher~~ greater than

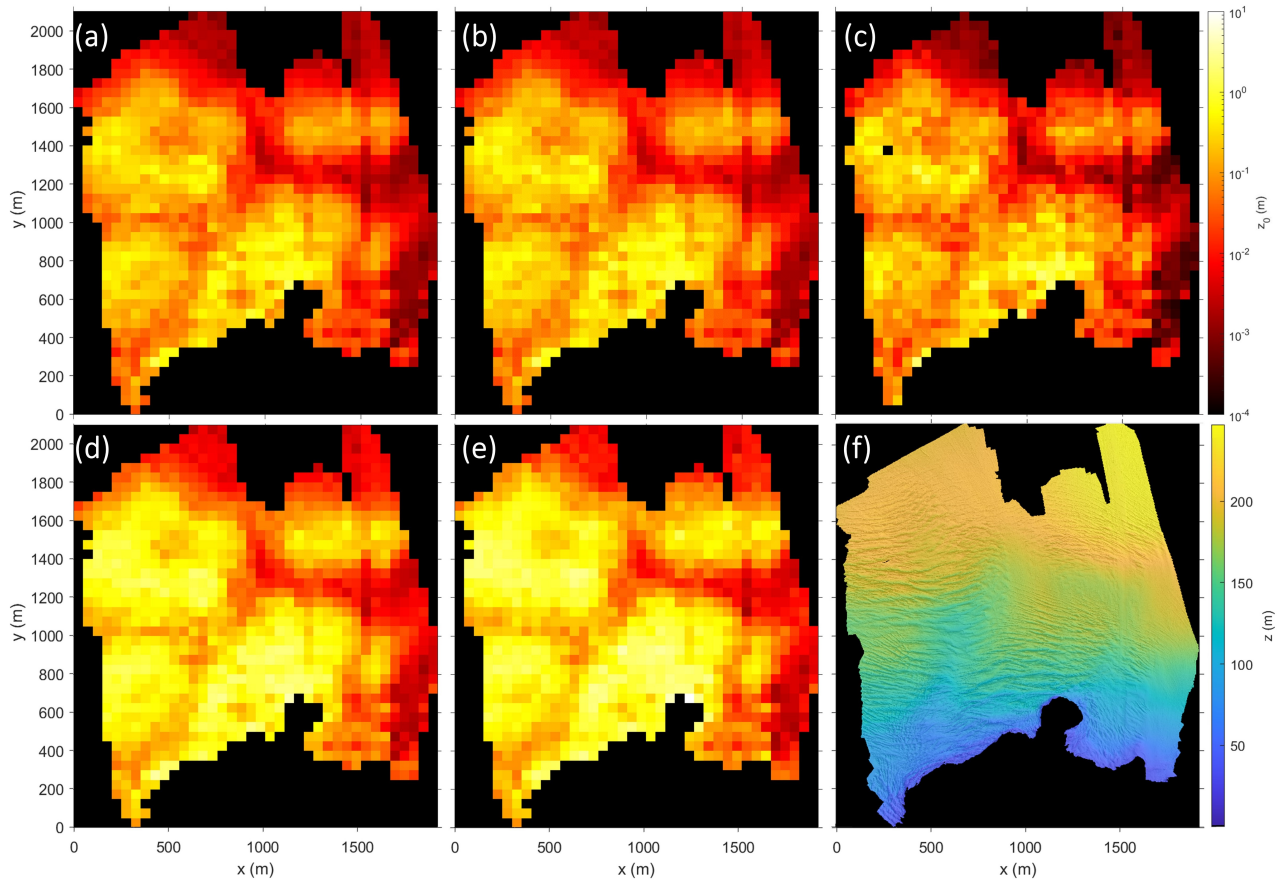


**Figure 4.** Variability of  $z_0$  values for Nordenskiöldbreen (2019) depending on the calculation models Smith (a), Chambers (b), Fitzpatrick (c), Munro (d) and Lettau (e) for a sub-grid size of  $50 \text{ m} \times 50 \text{ m}$  and a down-glacier wind direction. Graph (f) shows the DEM with the underlaid hillshade layer.

those of the Munro model and Chamber  $z_0$  values ~~higher~~<sup>greater</sup> than those of the Smith model (see also Table 4). The three models of the raster method provide sub-grid  $z_0$  values of about 0.001 m for slightly crevassed areas and up to 1 m for really heavily crevassed areas. The same sub-grids calculated with the two transect methods produced  $z_0$  values which are locally up to one order of magnitude larger. Table 4 illustrates the down-glacier and cross-glacier (left-to-right) mean  $z_0$  values for all glaciers and models. Table 4 also shows that average  $z_0$  values across the glacier vary almost up to half an order of magnitude between the models. In summary, despite the clear relative agreement between the models, the estimated magnitude of the  $z_0$  values varies substantially between the models - especially between the raster and transect method models. This might be explained by the fact, that the transect method does not account for sheltering of an obstacle (Smith et al., 2016). The raster method on the other hand assumes the areas below the detrended plane to be effectively sheltered. This plane indicates how

**Table 4.** Overview of mean  $z_0$  values (m) for each glacier and model either for the down-glacier or cross-glacier (left-to-right) wind direction.

Glacier	Wind Direction	Smith	Chambers	Fitzpatrick	Munro	Lettau
Nordenskiöldbreen 2019	Down-glacier (m)	0.129	0.151	0.126	0.393	0.496
	Cross-Glacier (m)	0.039	0.046	0.036	0.124	0.155
Tunabreen	Down-glacier (m)	0.223	0.271	0.196	0.709	0.883
	Cross-Glacier (m)	0.092	0.113	0.090	0.305	0.363
Heuglinbreen	Down-glacier (m)	0.150	0.187	0.175	0.415	0.424
	Cross-Glacier (m)	0.045	0.054	0.051	0.141	0.156
Fridtjovbreen	Down-glacier (m)	0.082	0.098	0.115	0.248	0.276
	Cross-Glacier (m)	0.028	0.034	0.039	0.090	0.094
Nordenskiöldbreen 2020	Down-glacier (m)	0.231	0.276	0.213	0.706	0.867
	Cross-Glacier (m)	0.052	0.062	0.050	0.172	0.212

far the effective turbulent mixing advances into the crevasses and the corresponding  $z_0$  values are expected to be lower if the sheltering effect is considered (Nicholson et al., 2016).

210 **3.2 Wind direction variability**

Figure 5 illustrates the map of Fridtjovbreen with  $z_0$  values obtained with the Smith method for all four cardinal-wind directions. The results show that  $z_0$  values are higher for wind directions that face the crevasses perpendicularly (i.e. up- and down-glacier) and lower for wind that blow parallel to the elongated crevasse features (i.e. cross-glacier). The two cross-glacier (up- and down-glacier, respectively) wind directions lead to very similar  $z_0$  values since they are both calculated on the same transect but from opposing wind directions. Since crevasses are mainly oriented perpendicular to the glacier flow direction, the mapped areas show a strongly anisotropic pattern of the glacier surface. This wind dependency effect is visible on all five applied models and is independent of the roughness element size. However, Fig. 5 illustrates that larger roughness elements (i.e. area, which can be found close to the glacier front and crevassed area in the centre of Fridtjovbreen) for instance, present a stronger wind dependency because they vary more strongly with changing wind directions (from dm to m scale) compared to areas that are less crevassed (e.g. like on the upper part of Fridtjovbreen (similar  $z_0$  values in mm scale for all wind directions)).

225 Additionally, Fig. 6 shows the boxplot graph of  $z_0$  estimations-estimates illustrating the wind direction dependency of  $z_0$  values on Fridtjovbreen. The boxplot  $z_0$  medians of all models vary in a range of 0.012 m to 0.037 m for crosswind directions and 0.058 m to 0.2 m for up- and down-glacier wind systems. The mean and median values between up- and down-glacier wind systems (left-to-right and right-to-left crosswinds, respectively) never differ more than 10 % and only rarely more than 5 % independent-independently of the chosen model or glacier. In summary, the wind direction has a large impact on the resulting aerodynamic roughness length values. Its effect on average or median  $z_0$  values slightly exceeds the model variability. Locally, however, both parameters-mean and median  $z_0$  estimates can vary about one order of magnitude with changing wind direction.

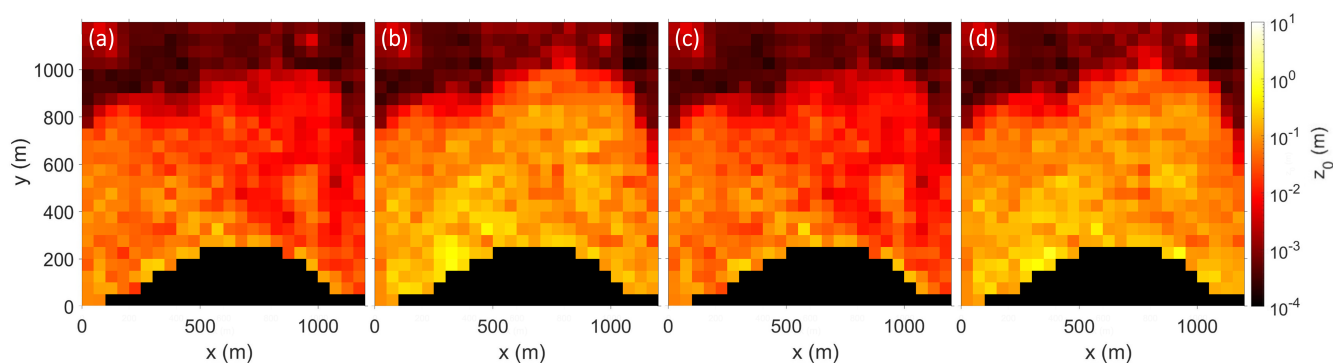


**Figure 5.** Variability of  $z_0$  values for Fridtjovbreen depending on the wind direction for a sub-grid size of 50 m calculated with the Smith model. Winds blowing across the glacier either from the left-to-right (a) or right-to-left (c) produce smaller  $z_0$  values than down- (b) or up-glacier (d) wind systems.

### 3.3 Glacier variability

~~Variability of  $z_0$  values for the glaciers Tunabreen (a) and Heuglinbreen (b) calculated with the Smith model for a down-glacier wind direction and a sub-grid size of 50 m.~~

All glaciers showed a similar range of  $z_0$  values with decimeter to meter scale for heavily crevassed areas and ~~millimeter~~ millimeter to centimeter scale for less crevassed areas (see Fig. 4, 5 and 7). However, the results of Table 4 show that the mean  $z_0$  values for the Smith model and down-glacier wind direction are somewhat larger on Tunabreen (0.223 m) and the extract of Nordenskiöldbreen mapped in 2020 (0.231 m) compared to the other glaciers. The same mean  $z_0$  values on Nordenskiöldbreen measured in 2019 are lower, with only 0.129 m. Heuglinbreen (0.15 m) and especially Fridtjovbreen (0.082 m) show lower mean  $z_0$  values than the glaciers mentioned above. Nevertheless, all the ~~observed patterns recognized in the investigations of~~ patterns found in this study (e.g. ~~impact of between~~ wind direction or sub-grid size ~~on and the~~  $z_0$  values) are independent of the ~~chosen~~ glacier and vary (if even) only in magnitude rather than relative patterns in between the glaciers.

On a side note, it is interesting to study the results of Nordenskiöldbreen 2019 and 2020 in more detail. The comparison provides insights on the inter-annual temporal variability of  $z_0$  values for two consecutive years. The mapped area in summer 2020 (one day of fieldwork) was smaller compared to the field campaign approximately one year earlier in 2019 (three days of fieldwork). Therefore, only the overlapping area has been used for the temporal variability investigation ~~and~~. Furthermore, for this particular comparison the DEM extract of Nordenskiöldbreen 2019 (0.17 m/px) was resampled to the resolution of the Nordenskiöldbreen 2020 DEM (0.22 m/px).  $z_0$  values on Nordenskiöldbreen ~~are were~~ very similar for the two consecutive years. The mean  $z_0$  value for the Smith model and down-glacier wind direction in 2019 ~~is with was, at~~ 0.25 m ~~only slightly higher, only slightly greater~~ than the corresponding value of 0.23 m ~~on at~~ the same area ~~but~~ one year later. The observations are in line with other studies (i.e. Fitzpatrick et al., 2019), which also did not observe a large difference in  $z_0$  estimates for

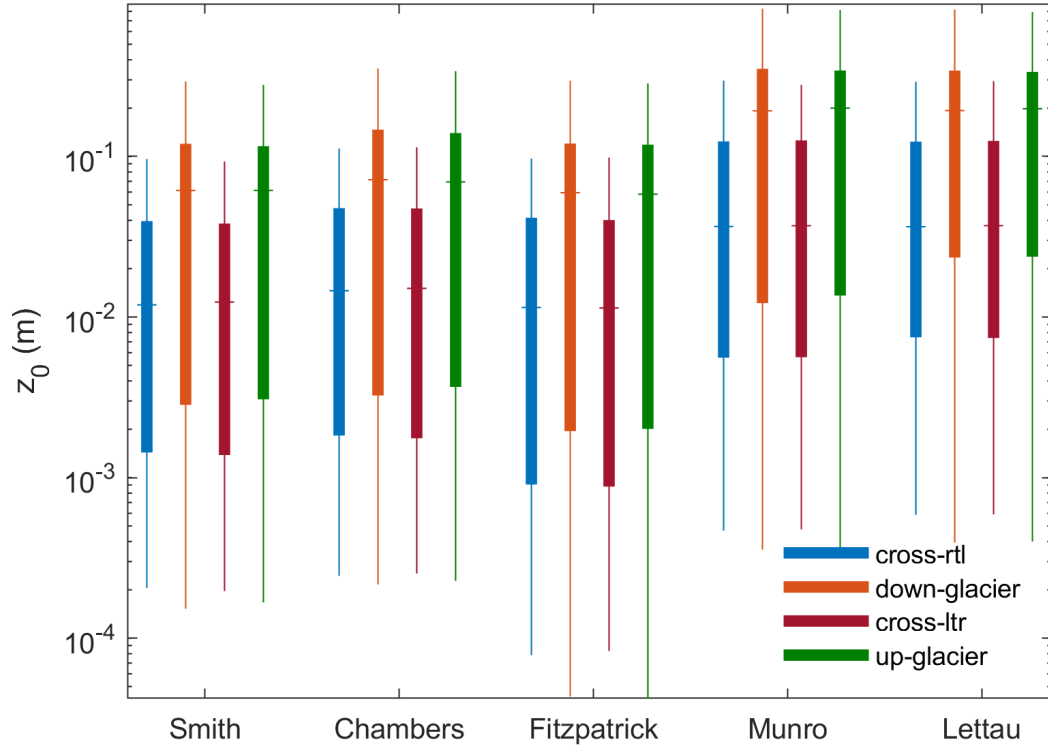


**Figure 6.** Boxplot visualization of sub-grid  $z_0$  values for all four wind directions and each applied model determined on Fridtjovbreen. The wind direction is either down- (orange) and up-glacier (green) or cross-glacier from right-to-left (blue) and left-to-right (red). Whiskers are visualizing the variability outside the upper and lower quartiles up to 1.5 times the interquartile range.

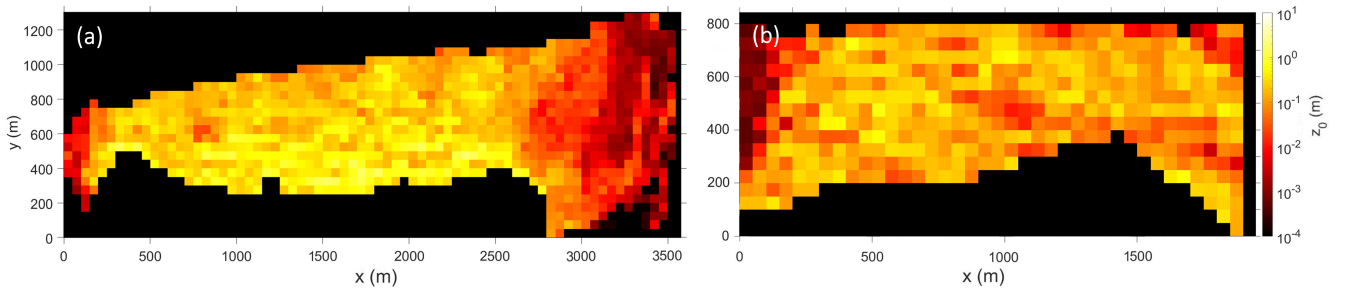


**Figure 7.** Variability of  $z_0$  values for the glaciers Tunabreen (a) and Heuglinbreen (b) calculated with the Smith model for a down-glacier wind direction and a sub-grid size of 50 m.

the same location ~~measured-in-over~~ two consecutive years. Relatively, the mean  $z_0$  values never deviated more than 20 % and mostly less than 10 % between the two years. ~~This small deviations in  $z_0$  values makes it hard to find the real reason for the decrease in  $z_0$  estimations. Nevertheless, the differences might be explained due to the fact that the data for the DEM 2020 was collected one month earlier. Thus, there might still be some snow bridges remaining in the crevasses what could have lowered the resulting aerodynamic roughness length.~~ In summary, the differences in ~~produced- $z_0$  estimations across the used estimates across the~~ models exceed the inter-annual temporal  $z_0$  variability by far, ~~independent-independently~~ of the model calculation.

### 3.4 Sub-grid size dependency

The mapped glacier areas were divided into sub-grids with a grid size of 50 m  $\times$  50 m to account for the spatial variability of  $z_0$  on the glacier. However, to investigate the grid size dependency of the sub-grids on  $z_0$  values, a small case study on the glacier Fridtjovbreen was conducted. The Smith model with a down-glacier wind direction was used to calculate aerodynamic roughness lengths for sub-grid sizes between 5 m and 150 m. Figure 8 illustrates the scale dependency of  $z_0$  values to the selected sub-grid size. The results show that a grid size of 5 to 10 m mostly produces  $z_0$  values in a scale of centimeters. Between sub-grid sizes of 10 and 50 m a higher grid size results in higher  $z_0$  values. From 50 m onwards, the  $z_0$  values are mostly ~~in the scale of decimeter~~ at the decimeter scale and do not change substantially. This behavior was also observed with the other models and for all wind directions. For small sub-grid sizes, the  $z_0$  values are likely representing microtopography rather than the macro-scale surface roughness of the crevasses.

Figure 9 summarizes the mean  $z_0$  results of the mentioned case study for the down-glacier wind direction. For all the models, the mean  $z_0$  values ~~increase-increased~~ by at least half order of magnitude between a sub-grid size of 5 m and 150 m. All models ~~show-showed~~ a similar pattern with strongly increasing  $z_0$  values for small grid sizes (5 m to 30 m) and only slightly increasing estimates afterwards. Grid sizes of 70 m or more ~~are loosing-lost~~ their strong scale dependency effect, leading to stable  $z_0$  ~~estimations~~ estimates. The same effect is visible on Fig. 8, where the chosen grid size of 50 m represents similar  $z_0$  values (colors) as the higher grid sizes for the same location while still providing a considerable grid resolution.

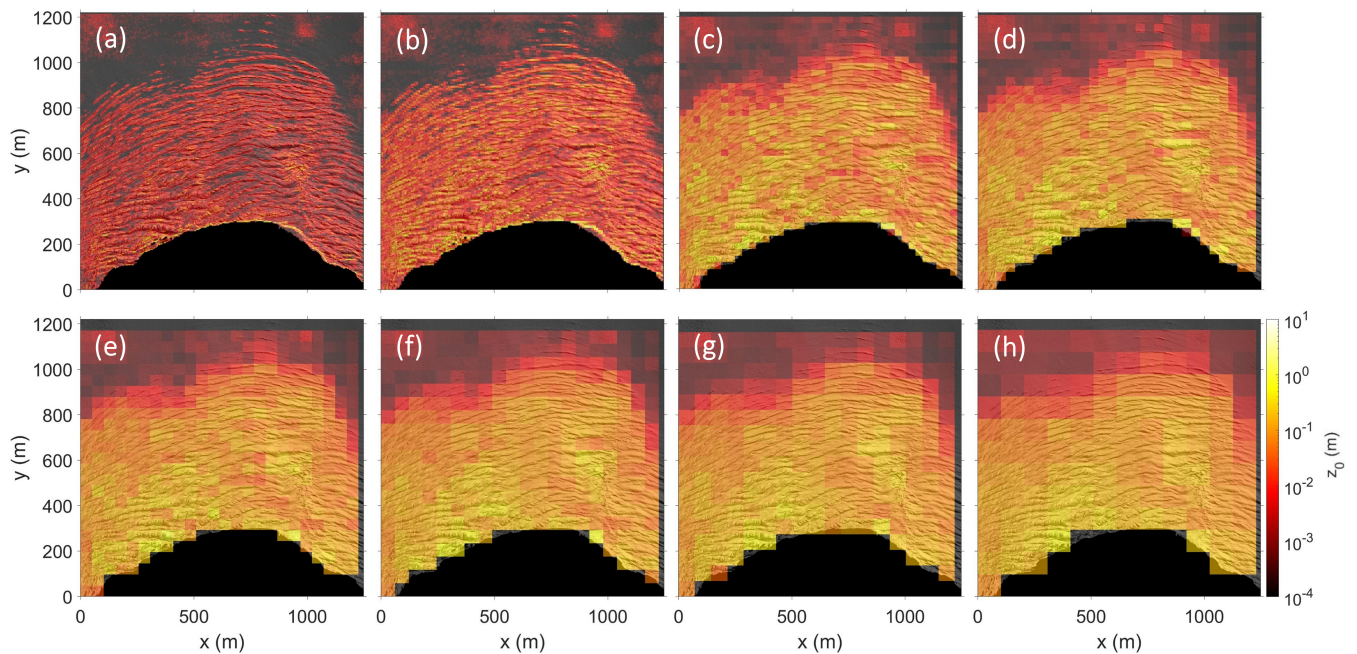


**Figure 8.** Scale dependent  $z_0$  values for the Smith model and down-glacier wind direction applied on Fridtjovbreen for sub-grid size resolutions of 5 m (a), 10 m (b), 30 m (c), 40 m (d), 50 m (e), 60 m (f), 70 m (g) and 100 m (h) with underlaid hillshade layer for orientation.

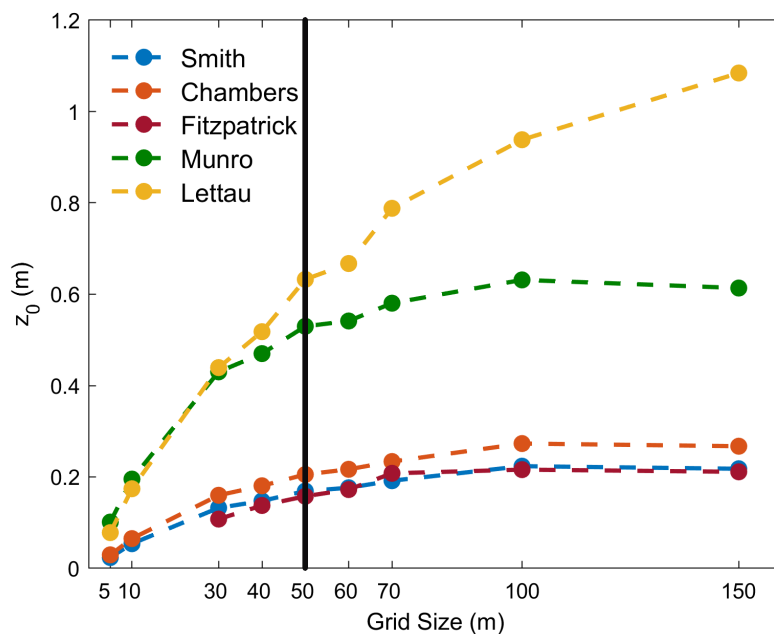


**Figure 9.** Scale dependency of mean  $z_0$  values for the five applied models and a down-glacier wind direction on Fridtjovbreen with chosen sub-grid sizes from 5 m to 150 m. The  $z_0$ -values are increasing with larger grid size. A vertical black line indicates the chosen grid size independent of 50 m which incorporates the chosen-model upper boundary of the average obstacle sizes between 30 and 50 m found on all glaciers (see Table 2).

## 4.1 Model inputs for aerodynamic roughness length estimation

### 4.1.1 Validation of digital elevation model accuracy

The obtained DEM resolution with the SfM-MVS method (about 0.25 m) was accurate enough to capture the large crevasse structures. Given the advantages of an UAV compared to other devices (e.g. ~~cheap price, applicable in low cost, applicable to~~ inaccessible areas (Hann et al., 2021)), this study shows that UAVs provide a reliable and effective way of data gathering for aerodynamic roughness length estimation on glaciers. Nevertheless, the depth of the crevasses must be seen as a minimum depth and the crevasses might penetrate further into the glacier than actually measured. This is due to snow-bridges or the lack of reflected light from the deep crevasses. The latter prevents the SfM-MVS methods ~~to correctly construct~~ from correctly constructing the deeper parts of the crevasse. Additionally, the lowest points of the crevasses are very narrow and may not be captured accurately (Ryan et al., 2015). However, in an aerodynamic context those narrow crevasses are not likely to have a significant influence on the heat exchange since they lie below the penetration depth of effective turbulent mixing (Nicholson et al., 2016). Equation 1 of Lettau (1969) and the transect methods do not define any penetration depth limit. The raster method however, assumes that effective roughness only depends on the roughness elements above the detrended plane level, which indicates how far the effective turbulent mixing advances into the crevasses.

In the scope of this study the ~~use of ground control points (GCPs) -~~ absence of GCPs was also considered. GCPs can significantly increase the georeferencing accuracy of the DEMs (Chudley et al., 2019). However, it was practically ~~not possible~~ impossible to place GCPs on the crevassed glacier surfaces ~~;~~ due to safety reasons. Therefore, the georeferencing information was provided only from the on-board GPS and the measurements of camera orientation (James et al., 2017). In other words, the positional accuracy of the DEM is limited by the internal GPS system of the UAV, which has a relatively low accuracy (Federman et al., 2017). However, ~~since~~ the objective of this study was not to obtain a high-accuracy DEM, but rather ~~to investigate the a precise DEM combined with a detrending approach for the investigation of the~~ effect of relative distances. Therefore, the given hover accuracy of  $\pm 1.5$  m horizontally and  $\pm 0.5$  m vertically for both UAVs (DJI, 2017, 2019) ~~;~~ was considered sufficient (Dachauer, 2020).

Nevertheless, a comparison with Sentinel-2 satellite data (ESA, 2020) revealed horizontal positioning errors (data not shown). The deviation was classified as a systematic offset (for more details see Dachauer (2020)). The detected small horizontal distortions of about 1.7 % (horizontal length deviation in % of DEM compared to the Sentinel-2 satellite image) mainly occurred on the ends of the DEMs. This is a typical feature appearing when only using nadir imagery and is related to self-calibration, because the reconstruction software is not able to derive the accurate radial lens distortion leading to a systematic 'doming' DEM deformation (James and Robson, 2014). However, a systematic error is of low significance for this study since only ~~a low the~~ relative accuracy of the roughness elements (i.e. distortion) influences the estimation of the aerodynamic roughness lengths. Furthermore, the influence of a small distortion of a few percents or several meters across the mapped area on the resulting  $z_0$  values is minor compared to other parameters such as wind direction, model calculation or scale dependency. ~~In~~

~~more detail~~For example, a distortion of 2 % led to a change in  $z_0$  of about 4 % (Dachauer, 2020). This means that the obtained DEMs in this study are a reliable data source to estimate the aerodynamic roughness length.

#### 305 4.1.2 Scale dependency

Many studies investigated and encountered the dependency of  $z_0$  ~~estimations~~estimates on the size of the sub-grid or the transect length (e.g. Fitzpatrick et al., 2019; Miles et al., 2017; Rees and Arnold, 2006) and reported that larger sub-grids or longer transects cause  $z_0$  values to increase (Chambers et al., 2020). Also the case study conducted on Fridtjovbreen data revealed that the  $z_0$  values increase with larger grid size ~~independent~~independently of the chosen glacier, model or wind  
310 direction. This can be explained by the fact that glaciers often have heterogeneous roughness elements (Quincey et al., 2017). In general, it needs to be considered that the selection of an appropriate grid size comes with a large potential uncertainty. To find the most meaningful grid size a comparison with independent methods like aerodynamic wind profiles is recommended (Chambers et al., 2020). Since this option was not available in our study, the validity of the chosen grid size has been evaluated theoretically. The grid size in our models ~~is correlated~~corresponds to the ground area  $S$ , whose definition requires the grid size  
315 to be the size of one individual roughness element (Lettau, 1969), which is 30 m to 50 m (see Table 2). According to ~~the theory of~~ Smith (2014), the definition of 'roughness' is related to the grid scale that separates the grain roughness (representing the texture of a roughness element) and the form roughness (corresponding to the form drag of the roughness element itself). The grid size, at which the transition from grain to form roughness occurs, provides a useful reference point and can be found ~~on~~  
as a kink in the trend line of a figure plotting  $z_0$  values against grid sizes (Shepard et al., 2001; Smith, 2014). ~~In~~Accordingly,  
320 given the large roughness elements investigated in our study, ~~this transition the 'grain' roughness was assumed to belong to the texture on the crevasses. Thus, the transition from grain to form roughness~~ is again located somewhere between a sub-grid size of 30 m to 50 m (see Figure 9). Therefore, in this study the grid size of 50 m was ~~justified such that it is large enough to include chosen since it is the smallest resolution possible to still include the size of~~ an average obstacle ~~size and small enough to provide a considerable spatial resolution of  $z_0$  values across the glacier.~~ Typical  $z_0$  estimates for smooth glacier ice, which  
325 for instance can be found on the upper part of Fridtjovbreen, have a length of about 1 mm (Brock et al., 2006). The choice of a 50 m grid size can further be justified since Figure 8 shows that grid sizes below 30 m do not provide high enough values and therefore do not agree with literature values.

## 4.2 ~~Model outputs of~~ Estimated aerodynamic roughness length ~~estimation~~

### 4.2.1 Wind direction dependency

330 The wind direction has a large impact on the magnitude of the  $z_0$  values on glaciers since they ~~obtain~~contain many anisotropic roughness elements (Chambers et al., 2020). Our results confirmed this statement and further revealed that larger roughness elements in general present a stronger wind dependency (see Fig. 5). The wind dependency effect was additionally investigated

with the calculation of the anisotropy ratio  $\Omega$  (see Smith et al. (2006) for further explanation):

$$\Omega = \frac{z_{0\parallel} - z_{0\perp}}{z_{0\parallel} + z_{0\perp}}, \quad (2)$$

335 where subscripts  $\parallel$  and  $\perp$  denote parallel and perpendicular to the ice flow direction, respectively. Figure 10 illustrates a histogram of the sub-grid's  $\Omega$  values on Fridtjovbreen for the Smith (blue) and Munro (green) model. The results show that the sub-grid  $z_0$  values are strongly anisotropic all across the glacier whereas wind directions parallel to the flow direction are dominant (since values are mostly positive). Both the raster (here Smith model) and the transect ~~method~~methods (Munro) show a similar pattern with the highest frequency at the range of 0.4 to 0.7 (Smith) and 0.4 to 0.8 (Munro). Although Tunabreen has  
340 still mostly positive ratio values, it is the glacier with the least anisotropic behaviour of all investigated glaciers. The importance of wind direction can be observed in many studies (e.g. Fitzpatrick et al., 2019; Munro, 1989; Smith et al., 2016) and is found to be the strongest on ablation zones where elongated features like meltwater channels and crevasses are frequent. Thus, wind directions that face these features perpendicularly lead to higher  $z_0$  values due to an increased form drag (Fitzpatrick et al., 2019). ~~However, winds~~Winds are in general very likely to blow in direction of the mean slope angle or in a down-  
345 slope wind direction (e.g. Fitzpatrick et al., 2019; Karner et al., 2013). This is due to katabatically forced down-slope winds, which are common over the glacier terminus (Munro, 1989). ~~Therefore, the effect of roughness anisotropy on the variation of~~  
Nevertheless, Esau and Repina (2012) found the katabatically forced wind systems to be of less significance for polar tidewater glaciers. This highlights the influence and importance of wind direction on effective  $z_0$  ~~values and hence on turbulent heat~~  
~~exchange might not be that important in many cases, because not all four wind directions have the same likelihood to occur~~  
350 ~~(Fitzpatrick et al., 2019).~~ Furthermore, the wind direction dependency reveals the temporal variability of the aerodynamic roughness length due to changing wind directions from daily up to seasonal time scales.

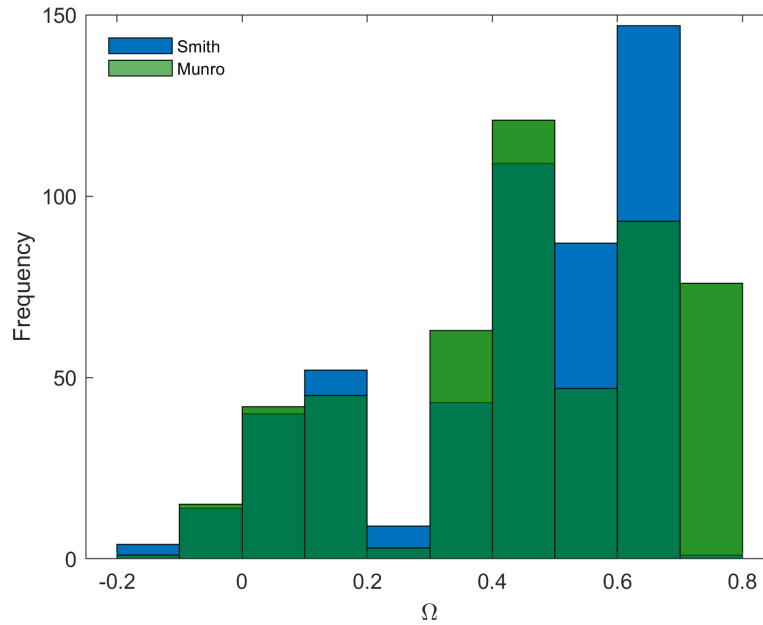


**Figure 10.** Anisotropy ratio values for the two models Smith (blue) and Munro (green) calculated for sub-grid  $z_0$  values on Fridtjovbreen. A positive ratio towards 1 means that parallel winds (up- and down-glacier) are dominant over perpendicular winds (cross-glacier).

#### 4.2.2 Variability across the glaciers

Since almost no values of  $z_0$  for heavily crevassed glaciers are available in the literature, the validation of the results of this study is difficult. The roughness elements investigated by previous studies (see Table 1) were smaller than the crevasses of this study. Therefore, it is expected that the  $z_0$  values obtained here should be larger. This was the case, although there was a significant spread of  $z_0$  values across the estimation models. The mean results in Table 4, and in particular their raster method results, fall mostly within the same order of magnitude. The range suggested by Fitzpatrick et al. (2019) fits most of the results from this study, across different methods and glaciers. Outside the field of glaciology, the heavily crevassed glaciers might most effectively be compared with villages, since buildings can have similar obstacle density and height. Accordingly, the  $z_0$  values for villages are about 0.2 - 0.4 m (Abbas et al., 2021) which lies within the range of estimated roughness values in this study.

In general, Tunabreen and Nordenskiöldbreen (especially the part mapped in 2020) show higher  $z_0$  values than Fridtjovbreen and Heuglinbreen. This is in good agreement with the average length and height of roughness elements estimated for each glacier in Table 2. The crevasses on Tunabreen and Nordenskiöldbreen are generally deeper and steeper than the crevasses on the other two glaciers. This might be explained by different dynamical behaviour, leading to higher  $z_0$  values. In general, a faster flowing glacier leads to more crevasses in the terminus area of the glacier and a larger area of crevassing (Błaszczuk et al., 2009). Additionally, Tunabreen was recently surging, ~~what~~ which usually leads to very chaotically aligned crevasses (Mansell

et al., 2012). Thus, these results are in line with the observation that the anisotropy ratio value  $\Omega$  is lowest on Tunabreen, as perfectly aligned roughness elements increase the anisotropy effect. However, comparing average  $z_0$  values among different glaciers is challenging because the mean  $z_0$  values depend a lot substantially on the mapped input area and therefore the size of included roughness elements. ~~The proportion of different glaciers that is heavily crevassed also varies markedly.~~

### 4.3 Model performance assessment

#### 4.3.1 ~~Transect and raster method comparison~~

~~All models managed to detect the large spatial variability on glaciers and to produce high relative  $z_0$  values in areas of large crevasses and low relative  $z_0$  values for non-crevassed areas. The  $R^2$  values among the models used in this study indicate that the  $z_0$  values were correlated, but do not provide any conclusion about the quality of the individual models. Therefore, as discussed by Miles et al. (2017), each model manages to provide an approximation of roughness in relative scales. The  $z_0$  results showed that the raster method produced values which are in general (locally up to one order of magnitude) lower than those calculated with the transect method. A series of studies (e.g. Chambers et al., 2020; Quincey et al., 2017; Smith et al., 2016, 2020) investigated the aerodynamic roughness length using both a transect and a raster method. However, no such study considered such heavily crevassed glaciers, which most likely makes the differences between the methods more obvious whilst also making it challenging to evaluate the model estimates. On rough or crevassed glacier ice, most of the mentioned studies also achieved lower  $z_0$  values with the raster method compared to the transect method and the effect usually increased for larger roughness elements. This might be because the transect method does not account for sheltering of an obstacle (Smith et al., 2016). Furthermore, the raster method neglects the frontal areas below the detrended plane, assuming that it would be effectively sheltered. This plane indicates how far the effective turbulent mixing advances into the crevasses and the corresponding  $z_0$  values are expected to be lower if the sheltering effect is considered (Nicholson et al., 2016).~~

#### 4.3.1 ~~Sheltering effect~~

~~The sheltering issue can be discussed from another perspective.~~ If the roughness elements on a plot are too densely packed, then the objects begin to interfere aerodynamically with each other (Rounce et al., 2015). They form a plateau-like new surface at their tops (Lettau, 1969) leading to a skimming flow. If this roughness density (frontal area divided by ground area) increases as far as is necessary to induce skimming flow, then the  $z_0$  values decrease (Grimmond and Oke, 1999). Accordingly, the results from the transect methods which are not considering any sheltering effects are likely to overestimate the roughness, especially for densely packed obstacles (Nicholson et al., 2016). Several studies (e.g. Nicholson et al., 2016; Rounce et al., 2015; Smith et al., 2016) used a roughness density threshold of 20 % to 30 % (as stated by Macdonald et al. (1998)) for Equation 1 of Lettau (1969) to still be valid. In our study, all glaciers were tested with the Smith model for their roughness density. Apart from some single heavily crevassed sub-grids close to the glacier front which exceed the threshold of 30 %, all glaciers are below the given threshold with mean roughness density values between 0.1 and 0.15 for each glacier, indicating no skimming

flow over the obstacles was likely. Therefore, this study ~~shows~~ assumes that the Lettau (1969) Equation 1 ~~can be assumed to~~  
400 ~~hold also~~ also holds on heavily crevassed tidewater glaciers with respect to the sheltering effect.

#### 4.3.1 Obstacle height

~~The~~ The Lettau formula is based on empirical experiments of systematically placed bushel baskets for roughness simulation. Transferring the simple relation onto heterogeneous and complex surfaces as found on the heavily crevassed tidewater glaciers might lead to some uncertainties. This is because the Lettau relation for the calculation of  $z_0$  strongly simplifies the complex  
405 surface roughness and its obstacle size, shape and density. A simplified representation of the surface roughness might fail to capture the complete range of aerodynamic processes. The Smith and Chambers models, as well as Munro and Lettau models, only differ in the definition of  $h^*$ . ~~Rounce et al. (2015) state that the~~ An appropriate definition of  $h^*$  is crucial since the obstacle height is the most important control parameter over the output of  $z_0$  (Nield et al., 2013b). Thus, the lack of a clear obstacle definition presents the main problem of the bulk method ~~approach introduced by Lettau (1969). Especially (Rounce et al., 2015)~~  
410 , especially in crevassed glacier areas, where an apparent base level is missing ~~, it is hard to define individual roughness elements and their according height (Nicholson et al., 2016; Smith et al., 2016).~~ Moreover, Nield et al. (2013b) state that the obstacle height is the most important control parameter over the output of  $z_0$ , meaning that an appropriate definition of  $h^*$  is crucial. Smith et al. (2016) on the one hand question the rationale behind the standard deviation approach. The authors state that any chosen obstacle height will be somewhat arbitrary and that their definition (i.e. mean height above detrended plane)  
415 ~~could be most meaningful on irregular ice surfaces. Chambers et al. (2020) on the other hand chose the standard deviation definition to preserve the influence of the larger roughness elements. (Nicholson et al., 2016).~~ To find out which model and which definition of  $h^*$  might perform best, a comparison with alternative measurement methods (e.g. wind profiles) would be necessary, as done in several studies (Fitzpatrick et al., 2019; Quincey et al., 2017; Smeets et al., 1999). For this study however, the area of interest was inaccessible and so this validation option was impossible. In any case, it clearly can be seen  
420 that the definition of  $h^*$  has a lower impact on the results than the ~~basic method itself~~ choice of the basic method (i.e. raster/-transect), which particularly affects the values of the silhouette area  $s$ . The definition of the ground area  $S$  which corresponds to the chosen grid size and the according profile length is a simple approximation of the real fetch footprint. However, the simplification allows estimation of  $z_0$  values for the four wind directions and additionally provides uniform parameterization throughout all glaciers and models. The widely adopted drag coefficient of Lettau (1969)  $c_d = 0.5$  corresponds to an average  
425 form drag effect on roughness elements. Its rationale is widely discussed since it does not necessarily hold for complex and heterogeneous locations, where drag may be large due to irregular density and shape of roughness elements. This might lead to a higher effective drag and therefore underestimated  $z_0$  values (Quincey et al., 2017).

#### 4.3.1 Overall model performance

In summary, the transect method is assuming isotropy, equal size and distribution of roughness elements and not considering  
430 ~~sheltering. None of those assumptions is particularly valid on heavily crevassed tidewater glaciers. Additionally, the transect method assumes tower-like roughness elements whereas in reality crevasses are getting narrower with depth. The raster method~~

is not making any of those assumptions. Furthermore, the raster method is making the best use out of the available dataset as every pixel value is considered for calculation (Smith et al., 2020). Despite the lack of any appropriate reference measurements, which clearly prevents a conclusion being drawn concerning best model performance, it can be stated that raster methods should ~~–at least theoretically– be more accurate.~~ With this being the case, we have demonstrated Turbulent fluxes already contribute a large fraction of surface ice melt (Fausto et al., 2016) and are supposed to have an even greater contribution to surface energy balance models under global warming (Smith et al., 2020). Thus, a high accuracy of estimated  $z_0$  values is desirable. The validation of the model estimates remains a big challenge due to the lack of reference values and it should be questioned whether the modelled  $z_0$  values are accurate enough for energy balance models. In general, an increase of  $z_0$  by one order of magnitude will more than double the value of turbulent fluxes (Brock et al., 2000). Therefore, whilst grid-size and model choice can contribute up to order of magnitude uncertainty in  $z_0$  values, it is far outweighed by the three orders of magnitude range in  $z_0$  observed in the present study. Spatial variability in  $z_0$  values caused by intense crevassing near the margin of tidewater glaciers therefore greatly exceeds the uncertainty introduced by modelling choices and can be constrained with sufficient accuracy through the methods pioneered here. Additionally, the relevance of further narrowing down the modelled range in the future depends a lot on the field of application. For large-scale, satellite-based investigations an average value between all models (e.g. 0.1 m) for heavily crevassed glacier areas might be a sufficiently accurate approximation. Small-scale investigations on individual glaciers on the other hand likely benefit from more accurate  $z_0$  estimates. It is here in particular, where our study shows that UAVs are the ideal platform for ~~applying this method~~ investigating aerodynamic roughness length.

## 5 Conclusions

The heavily crevassed terminus areas of the tidewater glaciers Fridtjovbreen, Heuglinbreen, Nordenskiöldbreen and Tunabreen were mapped with UAVs to build DEMs that revealed crevasse shape information. To take into account the spatial variability across the glacier, the DEM was divided into sub-grids of 50 m × 50 m, which was assumed to be large enough to include an average roughness element while still being small enough to account for the roughness variability across the glacier. Five different models (belonging to either the transect or the raster method) were applied to each DEM sub-grid to calculate the aerodynamic roughness length. The  $z_0$  ~~estimations~~estimates from the transect method ~~are~~were in general greater (up to one order of magnitude) than the raster method estimations. Wind direction and sub-grid size ~~have~~had a large impact on the  $z_0$  ~~estimations~~estimates, again producing a range of up to one order of magnitude for each parameter. Winds blowing parallel to the ice flow direction ~~produce~~produced larger  $z_0$  values than cross-glacier winds. The chosen sub-grid size presents a large uncertainty in aerodynamic roughness length estimation. The resulting  $z_0$  values are strongly scale dependent, such that a larger grid size leads to greater  $z_0$  values. If all parameters (i.e. model, wind direction, grid size) are included, the spread of the resulting  $z_0$  ~~estimations~~estimates is large, ranging from below one ~~millimeter~~millimeter (snow-covered, smooth glacier surface) up to several decimeters (heavily crevassed ice) or locally even more. Averaged  $z_0$  values for down-glacier wind directions varied from 0.08 m to 0.88 m depending on glacier and model. Nevertheless, all models managed to detect the same spatial variability across the glacier. The UAV approach allows several  $z_0$  values for each mapped glacier area to be derived,

465 which is crucial for heavily crevassed glaciers ~~;~~ since one value would be a poor representation of the real roughness across such a complex topography. Therefore, models can now incorporate distributed  $z_0$  ~~estimations~~estimates easily following UAV deployment, potentially leading to a better representation of turbulent heat fluxes and prediction of surface ice melt rates.

Spatial and temporal variability in crevassing, and a dependence on wind direction were found to extend the range of  $z_0$  values ~~found across on~~ tidewater glaciers. Variability caused by sub-grid size and model calculation assumptions reveal un-  
470 certainties which should be addressed by future investigations. Some degree of uncertainty also comes with the unsatisfactory georeferencing of the DEM in crevassed areas, because the inaccessible topography ~~sets~~imposes practical limitations, especially to the use of GCPs. Furthermore, future work should seek a scale-independent method for  $z_0$  calculation and also assess model performance using meteorological measurements (e.g. wind profiles) or computational fluid dynamics simulations. In a next step, a combination of high-resolution DEMs from UAVs for reference  $z_0$  values and satellite-based crevasse density  
475 estimates might approve valuable for future research.

*Code availability.* The codes used in this manuscript can be downloaded from [https://github.com/ArminDach/z0\\_UAVs](https://github.com/ArminDach/z0_UAVs).

*Data availability.* The data used in this manuscript can be downloaded from <https://doi.org/10.18710/JMWF3E>. Additional data can be obtained from the authors without conditions.

*Author contributions.* Conceptualization, AJH, RH and AD; data curation, RH; methodology, AD and RH; project administration, RH;  
480 formal analysis, AD; investigation, AD; visualization, AD; resources, RH and AJH; writing—original draft preparation, AD; writing—review and editing, AD and RH; supervision, RH and AJH. All authors have read and agreed to the published version of the manuscript.

*Competing interests.* The authors declare that they have no conflict of interest.

*Acknowledgements.* Fieldwork was funded by the Arctic Field Grant (RiS ID: 11148), provided by the Svalbard Science Forum (SSF) which is coordinated by the Research Council of Norway (RCN). The work is partly sponsored by the RCN through the Centre of Excellence  
485 funding scheme, project number 223254, AMOS, and project CLIMAGAS with project number 294764. Additionally, we much appreciate the help of Dr. Evan Stewart Miles by sharing his codes and knowledge.

## References

- Abbas, M. R., Bin Rasib, A. W., Abbas, T. R., Ahmad, B. B., and Dutsenwai, H. S.: Assessment of Aerodynamic Roughness Length Using Remotely Sensed Land Cover Features and MODIS, *IOP Conference Series: Earth and Environmental Science*, 722, 012015, <https://doi.org/10.1088/1755-1315/722/1/012015>, 2021.
- Agisoft LLC: Agisoft Metashape, <https://www.agisoft.com/>, 2020.
- Bhardwaj, A., Sam, L., Akanksha, Martín-Torres, F. J., and Kumar, R.: UAVs as remote sensing platform in glaciology: Present applications and future prospects, *Remote Sensing of Environment*, 175, 196–204, <https://doi.org/10.1016/j.rse.2015.12.029>, 2016.
- Błaszczyk, M., Jania, J. A., and Hagen, J. O.: Tidewater glaciers of Svalbard: Recent changes and estimates of calving fluxes, *Polish Polar Research*, 30, 85–142, 2009.
- Brock, B. W., Willis, I. C., Sharp, M. J., and Arnold, N. S.: Modelling seasonal and spatial variations in the surface energy balance of Haut Glacier d’Arolla, Switzerland, *Annals of Glaciology*, 31, 53–62, <https://doi.org/10.3189/172756400781820183>, 2000.
- Brock, B. W., Willis, I. C., and Sharp, M. J.: Measurement and parameterization of aerodynamic roughness length variations at Haut Glacier d’Arolla, Switzerland, *Journal of Glaciology*, 52, 281–297, <https://doi.org/10.3189/172756506781828746>, 2006.
- Casella, V. and Franzini, M.: Modelling steep surfaces by various configurations of nadir and oblique photogrammetry, in: *ISPRS Annals of Photogrammetry, Remote Sensing and Spatial Information Sciences*, vol. III-1, pp. 175–182, Prague, Czech Republic, <https://doi.org/10.5194/isprsannals-iii-1-175-2016>, 2016.
- Chambers, J. R., Smith, M. W., Quincey, D. J., Carrivick, J. L., Ross, A. N., and James, M. R.: Glacial Aerodynamic Roughness Estimates: Uncertainty, Sensitivity, and Precision in Field Measurements, *Journal of Geophysical Research: Earth Surface*, 125, 1–19, <https://doi.org/10.1029/2019JF005167>, 2020.
- Chappell, A. and Heritage, G. L.: Using illumination and shadow to model aerodynamic resistance and flow separation: An isotropic study, *Atmospheric Environment*, 41, 5817–5830, <https://doi.org/10.1016/j.atmosenv.2007.03.037>, 2007.
- Chudley, T. R., Christoffersen, P., Doyle, S. H., Abellan, A., and Snooke, N.: High-accuracy UAV photogrammetry of ice sheet dynamics with no ground control, *Cryosphere*, 13, 955–968, <https://doi.org/10.5194/tc-13-955-2019>, 2019.
- Dachauer, A.: Aerodynamic Roughness Length of Crevassed Tidewater Glaciers from UAV Mapping, Master Thesis, p. 100, <https://folk.ntnu.no/richahan/Publications/2020{ }Dachauer{ }Thesis.pdf>, 2020.
- DJI: Phantom 4 Pro/Pro+, User Manual v1.4, Tech. rep., 2017.
- DJI: Mavic 2 Enterprise Series, User Manual v1.8, Tech. rep., 2019.
- Ericson, Y., Falck, E., Chierici, M., Fransson, A., and Kristiansen, S.: Marine CO<sub>2</sub> system variability in a high arctic tidewater-glacier fjord system, Tempelfjorden, Svalbard, *Continental Shelf Research*, 181, 1–13, <https://doi.org/10.1016/j.csr.2019.04.013>, 2019.
- ESA: Copernicus Open Access Hub, <https://scihub.copernicus.eu/>, 2020.
- Esau, I. and Repina, I.: Wind climate in kongsfjorden, svalbard, and attribution of leading wind driving mechanisms through turbulence-resolving simulations, *Advances in Meteorology*, 2012, <https://doi.org/10.1155/2012/568454>, 2012.
- Fausto, R. S., Van As, D., Box, J. E., Colgan, W., Langen, P. L., and Mottram, R. H.: The implication of nonradiative energy fluxes dominating Greenland ice sheet exceptional ablation area surface melt in 2012, *Geophysical Research Letters*, 43, 2649–2658, <https://doi.org/10.1002/2016GL067720>, 2016.

- Federman, A., Santana Quintero, M., Kretz, S., Gregg, J., Lengies, M., Ouimet, C., and Laliberte, J.: UAV photogrammetric workflows: A best practice guideline, in: International Archives of the Photogrammetry, Remote Sensing and Spatial Information Sciences - ISPRS Archives, vol. 42, pp. 237–244, Ottawa, Canada, <https://doi.org/10.5194/isprs-archives-XLII-2-W5-237-2017>, 2017.
- 525 Fitzpatrick, N., Radić, V., and Menounos, B.: A multi-season investigation of glacier surface roughness lengths through in situ and remote observation, *The Cryosphere*, 13, 1051–1071, <https://doi.org/10.5194/tc-13-1051-2019>, 2019.
- Grimmond, C. S. B. and Oke, T. R.: Aerodynamic Properties of Urban Areas Derived from Analysis of Surface Form, *Journal of Applied Meteorology*, 38, 1262–1292, [https://doi.org/10.1175/1520-0450\(1999\)038<1262:APOUAD>2.0.CO;2](https://doi.org/10.1175/1520-0450(1999)038<1262:APOUAD>2.0.CO;2), 1999.
- Hagen, J. O., Liestøl, O., Roland, E., and Jørgensen, T.: *Glacier Atlas of Svalbard and Jan Mayen*, Norsk polarinstitutt, Oslo, 1993.
- 530 Hann, R., Altstädter, B., Betlem, P., Deja, K., Dragańska-Deja, K., Ewertowski, M., Hartvich, F., Jonassen, M., Lampert, A., Laska, M., Sobota, I., Storvold, R., Tomczyk, A., Woźtysiak, K., and Zagórski, P.: Scientific Applications of Unmanned Vehicles in Svalbard, SESS report 2020, Svalbard Integrated Arctic Earth Observing System, <https://doi.org/10.5281/ZENODO.4293283>, 2021.
- Hanssen-Bauer, I., Førland, E. J., Hisdal, H., Mayer, S., Sandø, A. B., Sorteberg, A., Adakudlu, M., Andresen, J., Bakke, J., Beldring, S., Benestad, R., Bilt, W., Bogen, J., Borstad, C., Breili, K., Breivik, Ø., Børsheim, K. Y., Christiansen, H. H., Dobler, A., Engeset, R., Frauenfelder, R., Gerland, S., Gjeltén, H. M., Gundersen, J., Isaksen, K., Jaedicke, C., Kierulf, H., Kohler, J., Li, H., Lutz, J., Melvold, K., Mezghani, A., Nilsen, F., Nilsen, I. B., Nilsen, J. E. Ø., Pavlova, O., Ravndal, O., Risebrobakken, B., Saloranta, T., Sandven, S., Schuler, T. V., Simpson, M. J. R., Skogen, M., Smedsrud, L. H., Sund, M., Vikhamar-Schuler, D., Westermann, S., and Wong, W. K.: Climate in Svalbard 2100, in: Norwegian Centre for Climate Services (NCCS), p. 105, The Norwegian Centre for Climate Services (NCCS), 2019.
- 535 Hock, R.: Glacier melt: A review of processes and their modelling, *Progress in Physical Geography*, 29, 362–391, <https://doi.org/10.1191/0309133305pp453ra>, 2005.
- Irvine-Fynn, T. D., Sanz-Ablanedo, E., Rutter, N., Smith, M. W., and Chandler, J. H.: Measuring glacier surface roughness using plot-scale, close-range digital photogrammetry, *Journal of Glaciology*, 60, 957–969, <https://doi.org/10.3189/2014JoG14J032>, 2014.
- James, M. R. and Robson, S.: Mitigating systematic error in topographic models derived from UAV and ground-based image networks, *Earth Surface Processes and Landforms*, 39, 1413–1420, <https://doi.org/10.1002/esp.3609>, 2014.
- 545 James, M. R., Robson, S., and Smith, M. W.: 3-D uncertainty-based topographic change detection with structure-from-motion photogrammetry: precision maps for ground control and directly georeferenced surveys, *Earth Surface Processes and Landforms*, 42, 1769–1788, <https://doi.org/10.1002/esp.4125>, 2017.
- Karner, F., Obleitner, F., Krismer, T., Kohler, J., and Greuell, W.: A decade of energy and mass balance investigations on the glacier Kongsvegen, Svalbard, *Journal of Geophysical Research Atmospheres*, 118, 3986–4000, <https://doi.org/10.1029/2012JD018342>, 2013.
- 550 Lettau, H.: Note on aerodynamic roughness-parameter estimation on the basis of roughness-element description, *Journal of applied meteorology*, 8, 828–832, 1969.
- Macdonald, R. W., Griffiths, R. F., and Hall, D. J.: An improved method for the estimation of surface roughness of obstacle arrays, *Atmospheric Environment*, 32, 1857–1864, [https://doi.org/10.1016/S1352-2310\(97\)00403-2](https://doi.org/10.1016/S1352-2310(97)00403-2), 1998.
- Mansell, D., Luckman, A., and Murray, T.: Dynamics of tidewater surge-type glaciers in northwest Svalbard, *Journal of Glaciology*, 58, 110–118, <https://doi.org/10.3189/2012JoG11J058>, 2012.
- 555 Miles, E. S., Steiner, J. F., and Brun, F.: Highly variable aerodynamic roughness length ( $z_0$ ) for a hummocky debris-covered glacier, *Journal of Geophysical Research: Atmospheres*, 122, 8447–8466, <https://doi.org/10.1002/2017JD026510>, 2017.
- Munro, D. S.: Surface roughness and bulk heat transfer on a glacier: comparison with eddy correlation, *Journal of Glaciology*, 35, 343–348, <https://doi.org/10.1017/S0022143000009266>, 1989.

- 560 Murray, T., James, T., MacHeret, Y., Lavrentiev, I., Glazovsky, A., and Sykes, H.: Geometric changes in a tidewater glacier in svalbard during its surge cycle, *Arctic, Antarctic, and Alpine Research*, 44, 359–367, <https://doi.org/10.1657/1938-4246-44.3.359>, 2012.
- Nicholson, L. I., Pętllicki, M., Partan, B., and MacDonell, S.: 3-D surface properties of glacier penitentes over an ablation season, measured using a Microsoft Xbox Kinect, *Cryosphere*, 10, 1897–1913, <https://doi.org/10.5194/tc-10-1897-2016>, 2016.
- Nield, J. M., Chiverrell, R. C., Darby, S. E., Leyland, J., Vircavs, L. H., and Jacobs, B.: Complex spatial feedbacks of tephra redistribution, ice melt and surface roughness modulate ablation on tephra covered glaciers, *Earth Surface Processes and Landforms*, 38, 95–102, <https://doi.org/10.1002/esp.3352>, 2013a.
- 565 Nield, J. M., King, J., Wiggs, G. F. S., Leyland, J., Bryant, R. G., Chiverrell, R. C., Darby, S. E., Eckardt, F. D., Thomas, D. S. G., Vircavs, L. H., and Washington, R.: Estimating aerodynamic roughness over complex surface terrain, *Journal of Geophysical Research: Atmospheres*, 118, 12 948–12 961, <https://doi.org/10.1002/2013JD020632>, 2013b.
- 570 Obleitner, F.: The energy budget of snow and ice at Breidamerkurjokull, Vatnajokull, Iceland, *Boundary-Layer Meteorology*, 97, 385–410, <https://doi.org/10.1023/A:1002734303353>, 2000.
- Quincey, D., Smith, M., Rounce, D., Ross, A., King, O., and Watson, C.: Evaluating morphological estimates of the aerodynamic roughness of debris covered glacier ice, *Earth Surface Processes and Landforms*, 42, 2541–2553, <https://doi.org/10.1002/esp.4198>, 2017.
- Rees, W. G. and Arnold, N. S.: Scale-dependent roughness of a glacier surface: Implications for radar backscatter and aerodynamic roughness modelling, *Journal of Glaciology*, 52, 214–222, <https://doi.org/10.3189/172756506781828665>, 2006.
- 575 Rounce, D. R., Quincey, D. J., and McKinney, D. C.: Debris-covered glacier energy balance model for Imja-Lhotse Shar Glacier in the Everest region of Nepal, *Cryosphere*, 9, 2295–2310, <https://doi.org/10.5194/tc-9-2295-2015>, 2015.
- Ryan, J. C., Hubbard, A. L., Box, J. E., Todd, J., Christoffersen, P., Carr, J. R., Holt, T. O., and Snooke, N.: UAV photogrammetry and structure from motion to assess calving dynamics at Store Glacier, a large outlet draining the Greenland ice sheet, *Cryosphere*, 9, 1–11, <https://doi.org/10.5194/tc-9-1-2015>, 2015.
- 580 Shepard, M. K., Campbell, B. A., Bulmer, M. H., Farr, T. G., Gaddis, L. R., and Plaut, J. J.: The roughness of natural terrain: A planetary and remote sensing perspective, *Journal of Geophysical Research: Planets*, 106, 32 777–32 795, <https://doi.org/10.1029/2000JE001429>, 2001.
- Smeets, C. J., Duynkerke, P. G., and Vugts, H. F.: Observed wind profiles and turbulence fluxes over an ice surface with changing surface roughness, *Boundary-Layer Meteorology*, 92, 101–123, <https://doi.org/10.1023/a:1001899015849>, 1999.
- 585 Smith, B. E., Raymond, C. F., and Scambos, T.: Anisotropic texture of ice sheet surfaces, *Journal of Geophysical Research: Earth Surface*, 111, 1–8, <https://doi.org/10.1029/2005JF000393>, 2006.
- Smith, M. W.: Roughness in the Earth Sciences, *Earth-Science Reviews*, 136, 202–225, <https://doi.org/10.1016/j.earscirev.2014.05.016>, 2014.
- Smith, M. W., Quincey, D. J., Dixon, T., Bingham, R. G., Carrivick, J. L., Irvine-Fynn, T. D. L., and Rippin, D. M.: Aerodynamic roughness of glacial ice surfaces derived from high-resolution topographic data, *Journal of Geophysical Research: Earth Surface*, 121, 748–766, <https://doi.org/10.1002/2015JF003759>, 2016.
- 590 Smith, T., Smith, M. W., Chambers, J. R., Sailer, R., Nicholson, L., Mertes, J., Quincey, D. J., Carrivick, J. L., and Stiperski, I.: A scale-dependent model to represent changing aerodynamic roughness of ablating glacier ice based on repeat topographic surveys, *Journal of Glaciology*, pp. 1–15, <https://doi.org/10.1017/jog.2020.56>, 2020.
- Uysal, M., Toprak, A. S., and Polat, N.: DEM generation with UAV Photogrammetry and accuracy analysis in Sahitler hill, *Measurement: Journal of the International Measurement Confederation*, 73, 539–543, <https://doi.org/10.1016/j.measurement.2015.06.010>, 2015.
- 595

- van Tiggelen, M., Smeets, P. C. J. P., Reijmer, C. H., Wouters, B., Steiner, J. F., Nieuwstraten, E. J., Immerzeel, W. W., and van den Broeke, M. R.: Mapping the aerodynamic roughness of the Greenland Ice Sheet surface using ICESat-2: evaluation over the K-transect, *The Cryosphere*, 15, 2601–2621, <https://doi.org/10.5194/tc-15-2601-2021>, 2021.
- Verhoeven, G.: Taking computer vision aloft - archaeological three-dimensional reconstructions from aerial photographs with photoscan, *Archaeological Prospection*, 18, 67–73, <https://doi.org/10.1002/arp.399>, 2011.